.1

Part V
Dynamics of the ISM

Contents

.2

Introduction

- References:
  Tielens 2005 Draine & Mc Kee, 2003, ARA&A, 31, 373
- Shocks are irreversible processes: ordered kinetic energy from stellar winds, supernova shock waves, etc ..., is converted into heat and chemical processes, with a concomitant entropy increase.
- Shocks are at the origin of the large-scale structure of the ISM and of the hot-shocked plasma phase ($\sim 10^6$ K).
- There are two broad types of shocks: J (jump) shocks and C (continuous) shocks. J-types are strong shocks that occur in all phases of the ISM, while C shocks are found in (magnetised) molecular clouds. The main difference between C and J shocks is the shock velocity. The minimum velocity for J-shocks is $\sim$40 km s^{-1}.

.3

1 J shocks

- In shocks the preferred reference system is that of the shock itself: the preshock gas flows towards the shock at the shock velocity v_s, while the postshock gas moves with the shock front, so has ~ 0 velocity relative to the shock.

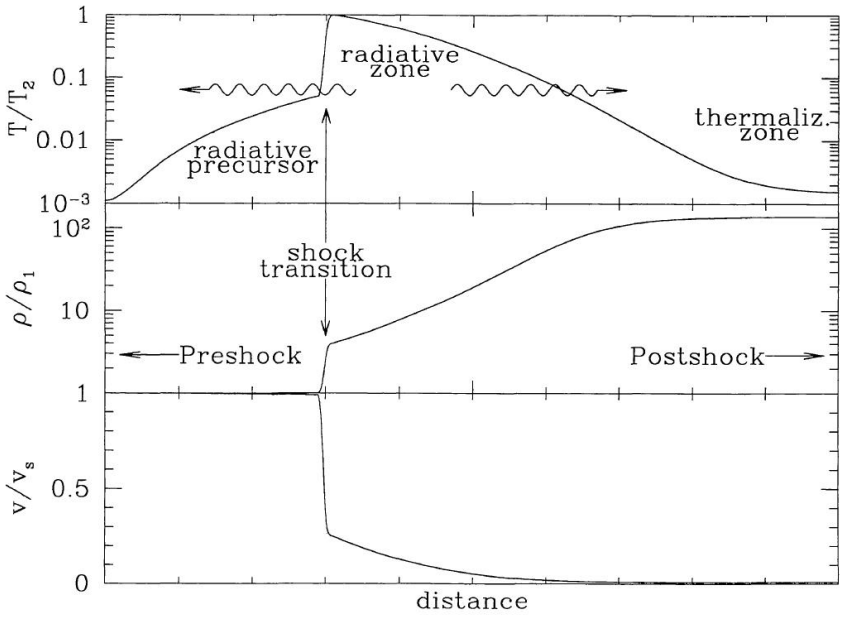

.4

Jump conditions

- J shocks are supersonic discontinuities. The speed of the shock can be expressed with the Mach number, $M = v_s/c_s$, where $c_s = \sqrt{\partial p/\partial\rho|_S}$ is the sound speed. For an adiabat $P \propto \rho^\gamma$ and the equation of state $P = \rho kT/\mu$, with $\gamma = 5/3$, $c_s = \sqrt{5/3kT/\mu}$.
- The fluid equations of motions take on simple forms when integrated across sharp discontinuities. These are the Rankine-Hugoniot jump conditons, which express the conservation of mass, momentum and energy flux.
- The flux of any scalar quantity per unit mass ϕ is $\phi\rho v$. Examples:
  - mass flux is ρv,
  - momentum flux is $(\rho v)v$ (v is the momentum per unit mass),
  - kinetic energy flux is $(\rho v)(v^2/2)$,
  - internal energy flux $(\rho v)(u/\rho)$, where $u = \sum_i (u_i + n_i I_i)$ is the internal energy per unit volume, and I_i is the binding energy of specie i, with number density n_i.

.5

Rankine-Hugoniot conditions

$$\rho_0 v_0 = \rho_1 v_1, \quad \text{mass}, \tag{1}$$

$$\rho_0 v_0^2 + P_0 = \rho_1 v_1^2 + P_1, \quad \text{momentum}, \tag{2}$$

$$\frac{1}{2}v_0^2 + \frac{u_0}{\rho_0} + \frac{P_0}{\rho_0} = \frac{1}{2}v_1^2 + \frac{u_1}{\rho_1} + \frac{P_1}{\rho_1}, \quad \text{energy}. \tag{3}$$

Eq. 3 derives from equating $P_0 v_0 - P_1 v_1$, the work done by the shock per unit time, to the net energy flux through the shock: $E_1 - E_0$, where

$$E_i = \rho_i v_i \left(\frac{1}{2} v_i^2 + \frac{u_i}{\rho_i} \right).$$

Note Eq. 3 expresses energy conservation for an adiabatic shock - without radiative losses, which are important for the evolution of the shock. .6

Solution of the jump conditions

For an ideal gas in an adiabatic shock, manipulation of the jump conditions gives (tarea):

$$\frac{P_1}{P_0} = \frac{2\gamma M^2}{\gamma+1} - \frac{\gamma-1}{\gamma+1}, \quad (4)$$

$$\frac{\rho_0}{\rho_1} = \frac{\gamma-1}{\gamma+1} + \frac{2}{\gamma+1}\frac{1}{M^2}, \quad (5)$$

$$v_i^2 = \frac{1}{\rho_i^2}(P_1 - P_0)\left(\frac{1}{\rho_0} - \frac{1}{\rho_1} \right)^{-1}. \quad (6)$$

For strong shocks, $M \gg 1$,

$$\frac{\rho_1}{\rho_0} = \frac{\gamma+1}{\gamma-1} \ (=4 \text{ for an ideal monatomic gas}), \quad (7)$$

$$P_1 = \frac{2}{\gamma+1}\rho_0 v_0^2 \ \left(= \frac{3}{4}\rho_0 v_0^2\right), \quad (8)$$

$$v_1 = v_0/4. \quad (9)$$

.7

Temperature rise at the shock front

For an ideal gas, Eq. 8 gives

$$T_1 = \frac{2(\gamma-1)}{\gamma+1}\frac{\mu v_0^2}{k} = \frac{3}{16}\frac{\mu}{k} v_0^2, \quad \text{for a monatomic gas.}$$

In a cosmic mix with a He abundance of -1 dex, $\mu/m_p = \sum n_i m_i / \sum n_i \approx 0.56$ for fully ionised gas , ≈ 1.3 for neutral gas, and ≈ 2.4 for molecular gas.

Thus, independently of the preshock phase,

$$T_1 \approx \frac{\mu}{m_p} 2.5\ 10^5 \left(\frac{v_0}{100 \text{ km s}^{-1}} \right)^2 \text{ K}$$

.8

Downstream conditions

Away from the (idealised) adiabatic shock front and into the postshock region, radiative losses decrease the temperature.

The flux of radiative energy $F_{\rm rad}$ varies as

$$\frac{d}{dz}F_{\rm rad} = n^2\Lambda - n\Gamma - 4\pi\kappa J,$$

where z is a coordinate along the shock propagation, n is number density, Λ and Γ are the cooling and heating rates, respectively, and J is the average intensity from other regions in the shock.

At some distance from the shock front, in a region which we may label as "2", the shocked gas will eventually relax to its preshock conditions, in region "0". We may apply the jump conditions to the 0–2 discontinuity, with an isothermal gas ($\gamma = 1$), so that Eq. 5 gives

$$\rho_2/\rho_1 = M^2.$$

We see shock waves are very compressive! .9

However, at very high temperatures the cooling rate is dominated by recombinations, with a rate $\Lambda \propto \sqrt{T}$, so that the cooling time scale, $\tau_{\rm cool} = kT/(n\Lambda(T)) \propto \sqrt{T}$.

Hence, if the shock is very strong $M \gg 1$, the postshock temperature can be arbitrarily high, and τ_{cool} correspondingly long - and possibly even longer than the lifetime of the shock (or the dynamical time scale). If so then the postshock region never relaxes, as is the case of the ISM hot-shocked by SNRs. .10

Precursor ionisation

In fast shock, if the postshock temperature reaches $\sim 10^5$ K, then H I is collisionally ionised and radiates in the Lyman continuum. The correspond ionising radiation overtakes the shock front and ionises the preshock gas.

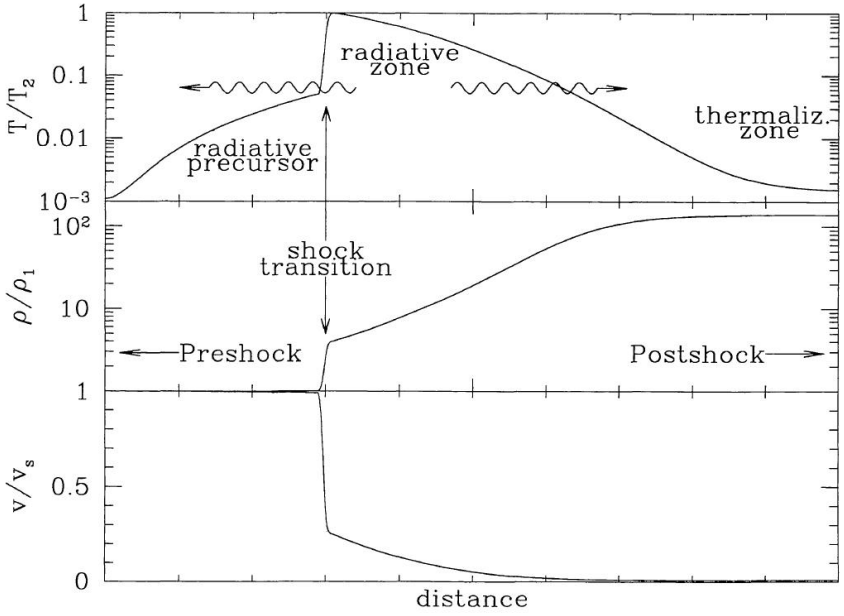

.11

J shock chemistry

- Shocks lead to dissociation/ionisation and eventually to molecule formation in the relaxation zone behind the shock front.
- The shock chemistry is radically different from the ion-molecule chemistry that occurs in quiescent dark clouds.
- Collisional H_2 dissociation occurs for gas at $> 10^5$ K, or shock velocities higher than 50 km s^{-1}.
- In the postshock region, with elevated temperatures, the chemistry taps on the gas internal energy to generate molecules via endothermic reactions. The key players in this chemistry are H, H_2 and O (assuming a cosmic mix with O>C).
  - If H_2 is not dissociated, then reactions with O leads to the formation of H_2O, so that the most abundant molecules are H_2, H_2O, CO, and O_2. Important trace molecules, characteristic of non-dissociating shocks, are CH^+, SiO, H_2S.
  - If H_2 is dissociated, loose H atoms collisionally dissociate molecules so that most of the gas is atomic (as expected from $\sim$ 1000 K gas).

.12

J shock spectra

- The spectra of non-ionising shocks reflect their chemistry.
- Ionising shocks lead to very hot, 10^6 K, gas and bright in X-rays. If the density is low, then the cooling timescale exceeds the shock lifetime, and columns are low, so that not much emission is found at UV-optical-IR wavelengths.
- If driven into dense media, ionising shocks may relax in the post-shock region, which is very compressed. The columns are then high enough for the detection of britght optical/IR collisionally excited fine structure lines.
- Since the relaxation zones dominate by mass the fully-ionised regions, the spectra of ionising shocks is dominated by low-excitation species, which are normally found in higher-ionisation stages in H II regions.

.13

- Two (among many) popular diagnostics for shock excitation versus photionisation are:
  - The ratio of [N II] $\lambda\lambda$6548,6584 to Hα λ6565 - [N II] is not as bright in H II regions than in shocks
  - The ratio [Fe II] 1.644μm / Brγ 2.166μm is high in shocks, because in H II regions Fe would be found in higher ionisation stages.

.14

2 C shocks

- For interstellar conditions, the magnetic field is "frozen" to matter. The magnetic flux $\Phi = \int_S \vec{B}.\vec{dS}$, where S is some surface tied to the fluid, is constant.
- When the gas is compressed perpendicular to $\vec{B}$, the field intensity increases so that $\Phi = SB$ is kept constant. As a result

$$B \approx \sqrt{n/1\ \mathrm{cm}^{-3}}\ \mu\mathrm{G}. \tag{10}$$

- Thus magnetic field intensities in dense molecular gas are high, and we must modify the shock equations to include the coupling of the magnetic field to the residual ionisation induced by cosmic ray ionizations.

.15

- Cosmic ray ionisation predicts an ionisation fraction of $x \approx 10^{-8} - 10^{-7}$, as observed (e.g. Wootten et al., 1979, ApJ, 234, 876).
- Most of the negative charge in molecular gas is found in PAH anions - they sweep out all the e^- ejected by the cosmic ray ionisation of H_2.
- Magnetised shocks are thus 2 fluid shocks: the ions, which directly couple to the magnetic field, and the neutrals, which lag behind the ions and are coupled to the field by collision and frictional drag with the ions.

.16

- The linearisation of the hydromagnetic equations shows that magnetised media sustain a wide variety of magnetosonic waves (an extension of sound waves).
- The type of Alfvén waves that is most relevant to shocks are transversal oscilations of the magnetic field lines, as in vibrating strings. Their speed is $v_A = B(4\pi\rho_i)^{-1/2}$, where ρ_i is the mass density of the ion fluid.
- The Alvén waves propagate the shock signal upstream, compressing the ions and dragging the neutrals. The wave energy is dissipated by ion-neutral friction, which raises the temperature.
- The shock front is merged with the relaxation layers. Thus magnetic shocks are continuous (C-shocks).

.17

Structure of C shock: shock width

- The characteristic length over which the neutral fluid velocity changes is $L \approx v_d/(n_i k_L)$, where $v_d = v_i - v_n$ is the ion-neutral drift velocity (which can be of the order of the shock velocity since the ions are first set in motion, and subsequently drag the neutrals - v_d values can be as high as $\sim$30 km s^{-1}), and $k_L = \langle w\sigma_{in}\rangle \approx 10{-}7\mathrm{cm}^3\ \mathrm{s}^{-1}$ is the Langevin rate (the number of ion-neutral collisions per ion per unit time, where w is ion-neutral relative velocities in the frame of the neutrals).

- As for the calculation in J-shocks, the maximum compression of ions is $(n_i/n_{i,0}) \approx v_s/v_A$, where v_s/v_A is an extension of the Mach number and $n_{i,0}$ is the pre-shock ion density. A working number for the ion-neutral drift velocity is half the shock velocity. Thus

$$L \approx \frac{v_A}{2 n_{i,0} k_L}.$$

- Assuming Eq. 10, we obtain $L \approx 1.1\ 10^5/(n_{i,0}k_L) \approx 10^{15}$ cm if the pre-shock proton density is 10^5 and the ionisation fraction is $x \sim 10^{-8}$.

.18

Structure of C shock: thermal balance

- Heating comes from the mechanical energy of the shock wave, hence

$$n\Gamma \approx \underbrace{\rho_0 v_s^2}_{\text{shock kinetic energy density}} \overbrace{(v_s/L)}^{\text{shock timescale}} .$$

- Shock cooling comes from H_2 rotational lines: $n^2\Lambda(T) = 2.5\ 10^{-33} n T^{3.82}$ erg cm^{-3} s^{-1}.
- Energy balance then gives the postshock temperature, $T \approx 1000 - 3000$ K for a 10 km s^{-1} shock with $L = 10^{15}$ cm and a factor of two density compression.

.19

Structure of C shock: detailed calculations

From Kaufman & Neufeld, 1996, ApK, 456, 611:

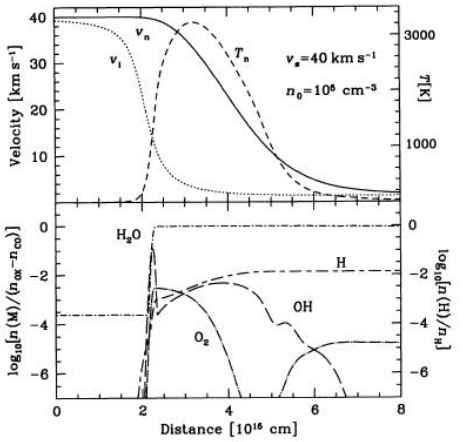

FIG. 1.—Shock profiles for a 40 km s^{-1} MHD shock propagating in gas of preshock H_2 density 10^5 cm^{-3}, and with a preshock magnetic field of 447 μG. The upper panel shows the flow velocities of the neutral fluid (v_n) and the ionized fluid (v_i) and the temperature of the neutral fluid (T_n) as a function of distance through the shocked region. The lower panel shows the abundances of the species O_2, OH, H_2O, and H [expressed relative to H nuclei in the case of H atoms (*right axis*) and relative to O nuclei not locked in CO in the case of O_2, OH, and H_2O (*left axis*)].

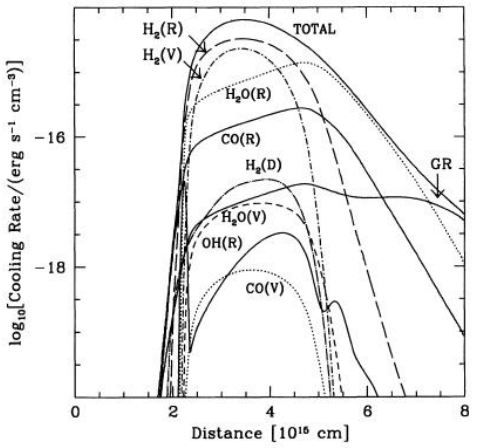

FIG. 2.—Cooling rate per unit volume attributable to vibrational (V) and rotational (R) emissions of CO, H_2, OH, and H_2O; from gas-grain collisions (GR); from H_2 dissociation [H_2(D)]; and from all processes combined (TOTAL). Results apply to a shock with v_s = 40 km s^{-1} and $n_0 = 10^5$ cm^{-3} and a preshock magnetic field of 447 μG.

.20

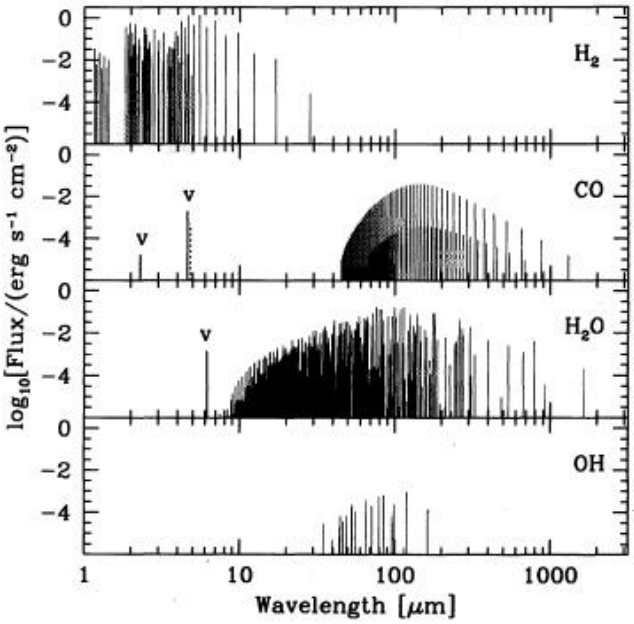

FIG. 4.—Line emission from a 40 km s^{-1} MHD shock wave propagating in gas with preshock density 10^5 cm^{-3} and with a preshock magnetic field of 447 μG. Results are shown for rotational and ro-vibrational transitions of H_2 (*top panel*), rotational transitions of ^{12}CO and ^{13}CO (*second panel*), rotational transitions of H_2O (*third panel*), and rotational transitions of OH (*bottom panel*). Also shown are the total fluxes in the ^{12}CO $v = 1$–0 and $v = 2$–0 vibrational bands near 4.6 μm and 2.3 μm (*solid lines*) and the $v = 2$–1 vibrational band near 4.6 μm (*dotted line*) and in the v_2 H_2O vibrational band near 6.2 μm (*solid line*).

.21

3 Supernova Remnants

References:

- Lequeux, "The interstellar medium" (like Spitzer 1978).
- Rohlfs & Wilson "Tools of Radioastronomy" (emphasis on the synchrotron diagnostic).
- Tielens.

.22

- There are three broad phases in the expansion of a SN shock wave:

  1. a phase of free expansion, where the density of the ejected material is much larger than the density of the surrounding medium. This phase ends $\sim$60 yr after the SN event. It has been studied extensively in extragalactic SNe.
  2. a phase of adiabatic expansion, where radiative losses are negligible, and where the temperature progressively cools through the work applied on the swept up ISM.

3. an isothermal phase, where the remnant's energy is lost by radiation, and which ends when the SNR shell velocity is of order of the velocity dispersion in the ISM ($\sim$ the sound speed, or 10 km s^{-1} in the diffuse ionised ISM at 10^4 K).

- SNRs of all types inject $\sim 10^{50}$ erg through a shocked shell driving into the ISM. SNe Ib/II may lead to *Plerions*: shell remnants filled with relativistic gas excited by a central pulsar.

.23

SNRs examples: Vela[1]

.24

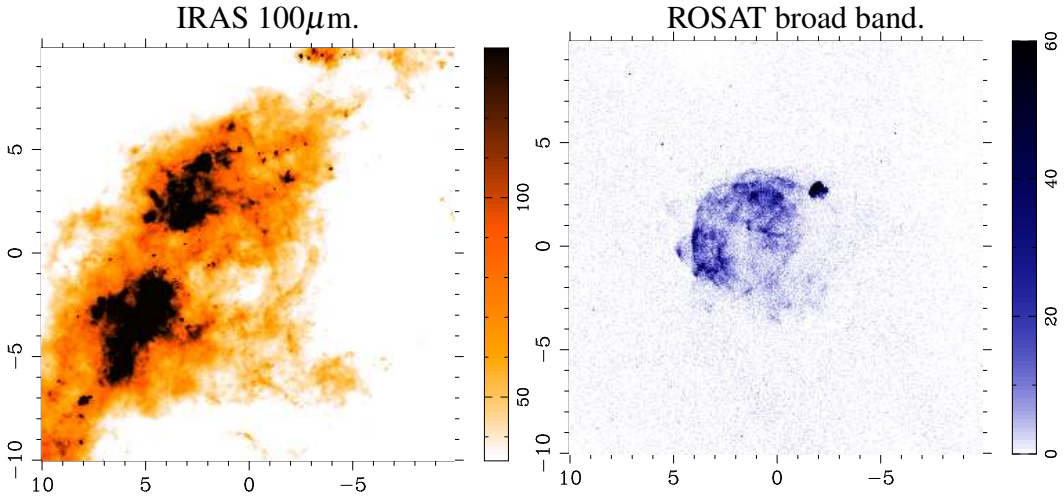

SNRs examples: Vela[2]

[1] G263.806−03.371

[2] Distance to Vela is $\sim$250 pc $\rightarrow$ 1 deg $\sim$ 5 pc

Hales et al. 2004, ApJ, 613, 977.
Bock et al., 1998, ApJ, 116, 1886.
Blondin et al. 2001, ApJ, 563, 806.

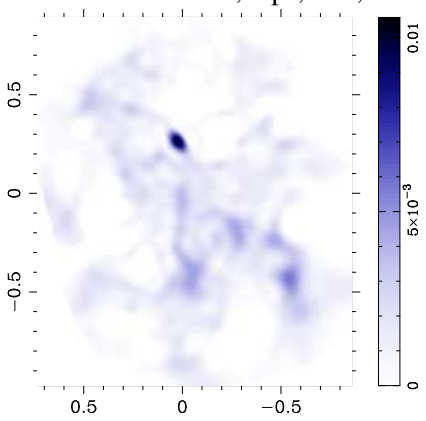

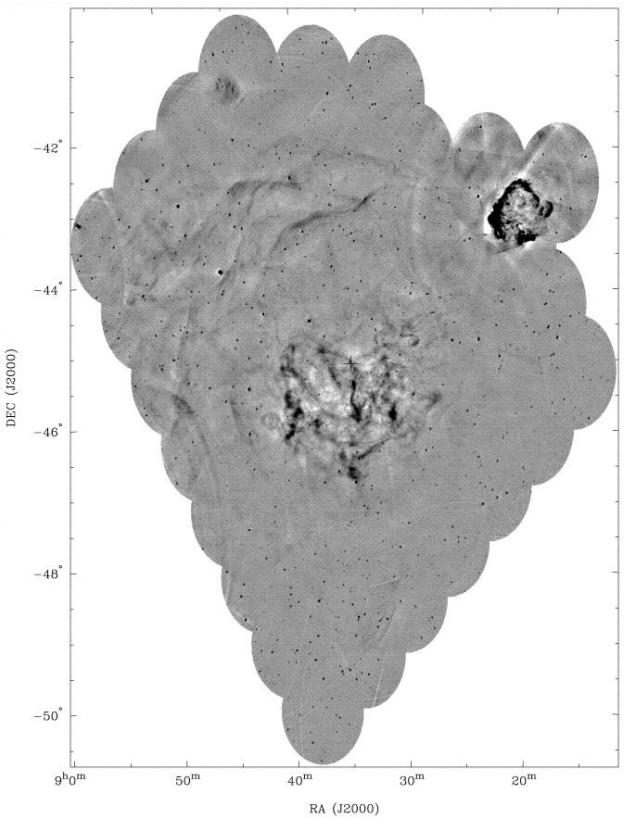

.25

SNRs examples: PWNe

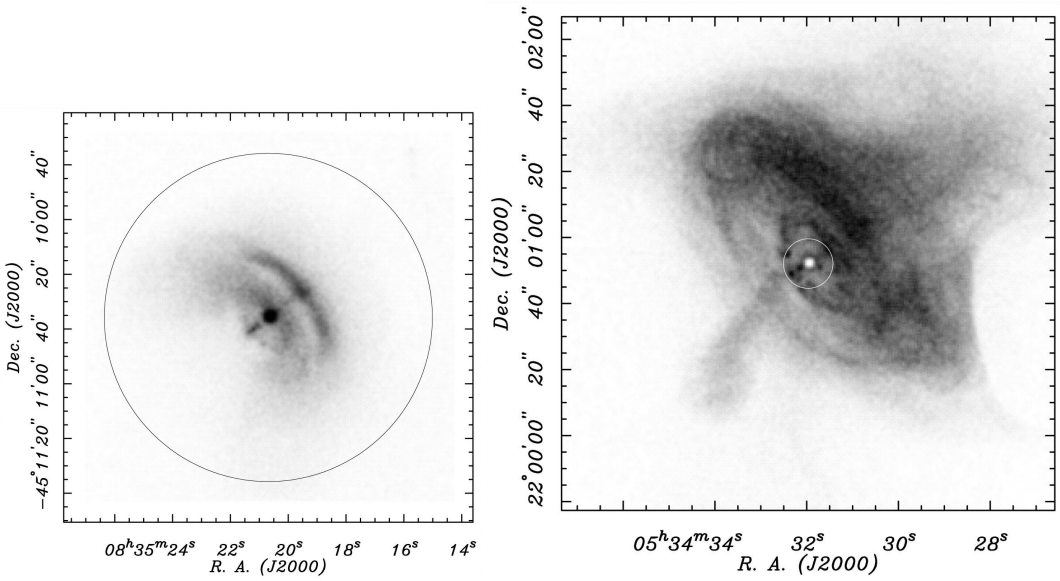

Helfand et al. (2001, ApJ, 556, 380) note that the ages of the Vela X (left) and Tau A (right) PWNe are very different (Vela X is $\sim 10^4$ yr, Blondin et al.). The circles have equal radii of $\sim$0.05 pc. The Vela X PSR radiates as a 1.7 10^6 K blackbody 10 km in radius, and the diffuse emission is synchrotron. That the arcs are not complete rings may be due to the head-light effect in the outflowing relativistic expansion.

.26

SNR free-expansion phase

- The SN event ejects the stellar envelope at $\sim 10^4$ km s^{-1}.
- For fully ionised gas the mean free path involves the Coulomb cross section of protons:

$$l = m^2 v^4/(Z^2 n e^4 \ln\Lambda), \text{ with } \Lambda = 1.3\ 10^4 T^{3/2}/n_e^{1/2}. \tag{11}$$

- At $v \sim 10^4$ km s^{-1}, the Coulomb cross section is so low that $l \sim 400$ pc for protons, so that they would escape the envelope.
- But a small magnetic field of only $\sim 1\mu$ G confines the protons to Larmor radii of only $\sim 10^{-8}$ pc. Thus the freely-expanding SNRs are MHD shocks.
- The free-expansion phase ends when the SNR expansion has swept up enough mass to slow down due to momentum conversation.
  This occurs when when the mass swept by the envelope, $\frac{4}{3}\pi r_s^3 \rho_0$, where ρ_0 is the surrounding density, is similar to the mass of the ejecta, $M_{\rm ej}$. For $n_0 \approx 1$ cm^{-3} and $M_{\rm ej} = 0.25$ M$_\odot$ (type Ia) we have $r_s = 1.3$ pc, which is reached only 60 yr after the explosion if the expansion velocity is 20000 km s^{-1}.

.27

SNR adiabatic (Sedov) expansion phase

- *Adiabatic* expansion means that the postshock temperature is so high that radiative losses are negligible. The mechanical SN energy E is constant.
- Sedov (1959) showed that adiabatic expansion is self-similar: its macroscopic parameters are related by power-laws (see Chap. A). In the Sedov phase,
  - the fraction of E that is thermal is $K_1 E$, with $K_1 = 0.72$,
  - the ratio $K_2 = P_1/\langle P\rangle = 2.13$, where P_1 is the pressure immediately behind the shock, and $\langle P\rangle$ is the average pressure inside the spherical remnant.

.28

Once the expansion slows down to, say, 1000 km s^{-1}, the magnetic energy density is negligible compared to the thermal energy density and we can use the J-shock results.

- With the above results from Sedov, and since for an ideal gas $\langle P\rangle = \frac{2}{3} K_1 E \frac{3}{4\pi r_s^3}$, we have $P_1 = KE/(2\pi r_s^3)$, where $K = K_1 K_2$.
- In the limit of a stron shock, $M \gg 1$, the Rankine-Hugoniot relations give $v_0 = \sqrt{\frac{4P_1}{3\rho_0}}$, and since the shock velocity $v_s \approx v_0$, we obtain

$$v_s = \sqrt{\frac{2KE}{3\pi r_s^3}}\ . \tag{12}$$

.29

- Integrating Eq 12,

$$r_s = \left(\frac{5}{2}\right)^{2/5} \left(\frac{2KE}{3\pi\rho_0}\right)^{1/5} t^{2/5},$$
$$= 0.26 \left(\frac{n_H}{\mathrm{cm}^{-3}}\right)^{1/5} \left(\frac{t}{\mathrm{yr}}\right)^{2/5} \left(\frac{E}{4\ 10^{50}\ \mathrm{erg}}\right)^{1/5} \mathrm{pc}.$$

- again, with the strong shock conditions Eq. 7 to 9,

$$T_1 = \frac{3}{16k}\mu m_H v_s^2 \qquad (13)$$
$$= 1.5\ 10^{11} \left(\frac{n_H}{\mathrm{cm}^{-3}}\right)^{-2/5} \left(\frac{t}{\mathrm{yr}}\right)^{-6/5} \left(\frac{E}{4\ 10^{50}\ \mathrm{erg}}\right)^{1/5} \mathrm{K}.$$

- we see that the T increases towards the centre, which reflects the neglect of radiative losses, and the fact that v_s was higher when the central layers were overtaken by the shock.

.30

Adiabatic expansion: thermal conductivity

- However, in the absence of strong magnetic fields, the Coulomb mean free path l (Eq. 11) is so high that diffusion is important, with thermal conductivity

$$\kappa = \frac{5}{3}\frac{kT}{\langle v_T \rangle} l\, n \frac{3k}{m}, \quad \text{with } \langle v_T \rangle = (3kT/m)^{1/2}. \qquad (14)$$

- Solving for the thermal balance including the heat flux $Q = -\kappa \nabla T$ leads to uniform temperatures in the SNR interior (Chevalier 1975, ApJ, 198, 355):

$$T \approx 1.4\ 10^{10} \left(\frac{n_0}{\mathrm{cm}^{-3}}\right)^{-1} \left(\frac{r_s}{\mathrm{pc}}\right)^{-3} \frac{E}{10^{51}\ erg}\ \mathrm{K}. \qquad (15)$$

- However, a finite magnetic field exists inside the remnant, so that the mean free path and the conductivity κ are reduced. The real temperature inside the remnant thus lies in between Eq. 13 and Eq. 15.

.31

Adiabatic expansion: reverse shock

- An more accurate (numerical) treatment shows that the transition between free and adiabatic expansion generates a reverse shock.
- The reverse shock propagates inwards, towards the centre of the ejected matter.
- Qualitatively, the reverse shock stems from the pressure increment behind the shock front. The finite radiative losses lower the temperature inwards and away from the shock front. Thus the sound speed decreases inwards, and the pressure perturbation right behind the (outer) shock turns into an inner, or reverse, shock.
- After the passage of the reverse shock the SNR expansion becomes truly adiabatic.

.32

Isothermal expansion

- When the postshock temperature falls below $T_1 \approx 10^6$ K, metals start recombining, and radiative cooling is strongly enhanced through line emission from ions of C, N and O.
- Energy is no longer conserved - rather, the expansion of the remnant is controled by momentum conversation.
- The transition into the isothermal phase occurs at an age of $\sim 10^4$ yr, for an ambient density $n_0 \sim 1$ cm^{-3}, a shell radius ~ 15 pc, and an expansion velocity of 85 km s^{-1}.

.33

- Momentum conservation requires that Mv_s is constant, where M is the ISM mass swept-up by the remnant:

$$\frac{4}{3}\pi r_s^3 \rho_0 v_s = \text{constant}.$$

- Integration then gives

$$r_s = r_{\rm rad}\left(\frac{8t}{5t_{\rm rad}} - \frac{3}{5}\right)^{1/4},$$

where $r_{\rm rad}$ and $t_{\rm rad}$ are the radius and age of the remnant at the start of the isothermal phase.

.34

Final mixing with the ISM

- When the age of the remant is of order 10^6 yr, its radius will be $\sim$40 pc, and $v_s \sim 10$ km s^{-1} - comparable to the sound speed of 10^4 K 'warm-ionised' ISM with $n_0 = 1$ cm^{-3}. Thus the remnant will no longer be supersonic, and will mix with the ISM.
- The efficiency η for the input of mechanical SN energy E into the ISM is

$$\eta = \frac{1}{2}M_f v_f^2/E,$$

where M_f and v_f are the final mass and velocity of the remnant. Lequeux (2005) shows that $\eta \approx 0.03$.

.35

4 Ionization fronts

Dynamics of H II regions

References:

- Lequeux, 2005, "The interstellar medium".
- Tenorio-Table & Bodenheimer, 1988, ARA&A, 26, 145
- Kaplan & Pikelner, 1970, "The interstellar medium".
- Tielens, 2005.

.36

Given an instantaneous proton density $n_p(t)$, ionisation equilibrium applied to a whole H II region gives its size, the Strömgren radius:

$$r_S = \left(\frac{3\pi}{4} \frac{S}{n_e n_p \alpha_2} \right)^{1/3}, \tag{16}$$

where S is the stellar-photon-luminosity in the Lyman continuum.

However the ionised gas is at a higher pressure than the surroundings. If the proton density is uniform, in the ionised region number densities are at least a factor of 2 higher than in neutral gas, and temperatures are $\sim 10^4$ K against $\sim 10-100$ K in the atomic/molecular gas. Thus H II regions are bound to expand, and their densities will decrease.

We will first quantify the dynamics of the ionisation front, and then consider the pressure wave propagating in the neutral gas as a precursor shock. .37

The ionisation front

In plane-parallel geometry, the equations describing the inertia of the front are:

$$\rho_0 v_0 = \rho_1 v_1, \quad \text{mass continuity} \tag{17}$$

$$\rho_0 v_0^2 + P_0 = \rho_1 v_1^2 + P_1, \quad \text{momentum equation.} \tag{18}$$

With

$$P_i = \rho_i kT/(\mu_i m_H), \quad \text{and,} \tag{19}$$

$$c_i = \sqrt{\gamma kT/(\mu_i m_H)}, \quad \text{the sound speed,} \tag{20}$$

we see that $P_i = c_i^2 \rho_i / \gamma$. .38

We can combine the above equations to give (tarea)

$$\frac{\rho_1}{\rho_0} = \frac{1}{2}\frac{c_0^2}{c_1^2}\left[(M^2+1) \pm \sqrt{(M^2+1)^2 - 4M^2 \frac{C_1^2}{C_0^2}} \right], \tag{21}$$

where $M = v_0/c_0$ is the Mach number of the ionisation front. The condition that the square root be real requires (tarea)

$$M^2 - 2M\frac{c_1}{c_0} + 1 > 0, \tag{22}$$

so that the only possible values for M are $M < M_D$ or $M > M_R$, where

$$M_R = \frac{c_1}{c_0}\left(1 + \sqrt{1 - \frac{c_0^2}{c_1^2}} \right), \tag{23}$$

$$M_D = \frac{c_1}{c_0}\left(1 - \sqrt{1 - \frac{c_0^2}{c_1^2}} \right). \tag{24}$$

.39

Since $T_0 \ll T_1$, $c_0 \ll c_1$ and

$$M_R \approx 2c_1/c_0, \tag{25}$$
$$M_D \approx c_0/(2c_1) \tag{26}$$

For either the 'R' or 'D' critical solutions, we have $M^2+1 = 2Mc_1/c_0$, so that Eq. 21 gives

$$\frac{\rho_1}{\rho_0} = M\frac{c_0}{c_1} = \frac{v_0}{c_1}. \tag{27}$$

The mass continuity equation then gives

$$v_1 = \rho_0 v_0/\rho_1 = c_1. \tag{28}$$

We see that for the critical values of M the downstream velocity of the gas is equal to the sound speed c_1. We will now turn to a detailed analysis of the critical solutions. .40

In plane-parallel geometry, the mass continuity equation gives

$$\rho_0 v_0 = \rho_1 v_1 = J, \tag{29}$$

where

$$J = \mu_0 m_H S \frac{e^{-\tau}}{4\pi r_s^2} \tag{30}$$

is the flux of hydrogen atoms through the front, and $\tau = n_d \sigma_d r_s$ is an average Lyman-continuum opacity mostly due to dust inside the H II region (in the on-the-spot approximation the contribution of opacity from residual atomic hydrogen is compensated by recombinations). .41

The momentum-conservation equation,

$$\rho_0 v_0^2 + P_0 = \rho_1 v_1^2 + P_1, \tag{31}$$

can be written

$$\rho_0 \left(\frac{kT_0}{\mu_0 m_H} + v_0^2 \right) = \rho_1 \left(\frac{kT_1}{\mu_1 m_H} + v_1^2 \right), \tag{32}$$

where we have neglected radiation pressure (¿ ojo?). .42

We will assume that the ionised gas behind the ionisation front expands freely into the H II region, at a velocity close to the sound speed (or close to the thermal rms speed) - this is exactly true for the critical 'R' or 'D' solutions:

$$v_1 \approx c_1 = \sqrt{\frac{\gamma k T_1}{\mu_1 m_H}}.$$

Substitution in the mass-continuity equation (Eq. 29) gives

$$\rho_1 = J/c_1, \tag{33}$$
$$\rho_0 = J/v_0. \tag{34}$$

.43

With Eq. 33 and 34, and using momentum conservation, Eq. 32, we obtain (tarea)

$$v_0 + \frac{1}{v_0}\frac{kT_0}{\mu_1 m_H} = (\gamma+1)\sqrt{\frac{kT_1}{\gamma\mu_1 m_H}}, \tag{35}$$

whose solution for v_0 is (tarea)

$$v_0 = \sqrt{\frac{(\gamma+1)^2 kT_1}{4\gamma\mu_1 m_H}} \pm \sqrt{\frac{(\gamma+1)^2 kT_1}{4\gamma\mu_1 m_H} - \frac{kT_0}{\mu_0 m_H}}. \tag{36}$$

Since $T_0 \ll T_1$,

$$v_0 = \sqrt{\frac{(\gamma+1)^2 kT_1}{4\gamma\mu_1 m_H}} \left\{ 1 \pm \left[1 - \frac{2\gamma}{(\gamma+1)^2}\frac{\mu_1}{\mu_0}\frac{T_0}{T_1} \right] \right\}. \tag{37}$$

.44

We see that we have two broad families of solutions, corresponding to each sign in Eq. 37.

- For the plus sign, the factor in curled brackets $\{...\}$ can be approximated to 1 for $T_0 \ll T_1$, so that
$$\frac{\rho_1}{\rho_0} = \frac{v_1}{v_0} = \frac{\gamma+1}{\gamma},$$
so that $\rho_1 > \rho_0$. This is called a *compression wave*, or the R solution (R is for rarefied gas, since the fronts meets gas of lower density).
- For the minus sign, we go to first order in T_0/T_1 and obtain (tarea)
$$\frac{\rho_1}{\rho_0} = \frac{v_1}{v_0} = \frac{1}{\gamma+1}\frac{\mu_1 T_0}{\mu_0 T_1},$$
so that $\rho_1 \ll \rho_0$. This is called a *rarefaction wave*, or the D solution (D is for dense gas, since the fronts meets gas of higher density).

.45

In order to estimate the temperature in the ionised gas behind the front, T_1, we use the conservation of energy (cf. Eq. eq:energy),

$$\rho_0 v_0 \left[\overbrace{\frac{\gamma kT_0}{(\gamma-1)\mu_0 m_H}}^{(u_0+P_0)/\rho_0} + \frac{1}{2}v_0^2 \right] = \rho_0 v_0 \left[\frac{\gamma kT_0}{(\gamma-1)\mu_0 m_H} + \frac{1}{2}v_0^2 \right] - \varepsilon_0 J, \tag{38}$$

where ε_0 is the mean energy per photoelectron (instantaneously behind the front we neglect radiative cooling, which is important for the subsequent mixing of the ionised gas). Using mass and momentum conservation, Eq. 29 and 32, we obtain

$$v_0^2 = \frac{\gamma+1}{\gamma-1}\frac{kT_1}{\mu_1 m_H} - \frac{2\gamma}{\gamma-1}\frac{kT_0}{\mu_0 m_H} - \frac{\varepsilon_0}{m_H}. \tag{39}$$

We can then obtain T_1 given T_0 by equating Eq. 37 and 39. .46

In summary,

- D-critical fronts, $\rho_0 > \rho_1$.

$$\begin{aligned} T_1 &= \tfrac{\gamma-1}{\gamma(\gamma+1)}\tfrac{\mu_1\varepsilon_0}{k}, \qquad v_0 = \tfrac{\mu_1 T_0}{\mu_0 T_1}\sqrt{\tfrac{(\gamma-1)\varepsilon_0}{(\gamma+1)^3 m_H}}, \\ \tfrac{\rho_1}{\rho_0} &= \tfrac{1}{\gamma+1}\tfrac{\mu_1 T_0}{\mu_0 T_1}, \qquad \rho_0 = J\sqrt{\tfrac{(\gamma+1)^3}{\gamma-1}\tfrac{m_H^3}{\varepsilon_0}}. \end{aligned} \tag{40}$$

  With $\gamma = 5/3$[3], we obtain $v_0 \approx 0.2$ km s^{-1}, $\rho_1/\rho_0 \approx 1/100$, and if $T_0 \sim 1000$ K then $T_1 \sim 3000 - -6000$ K. Further downstream the gas will heat to its equilibrium value of 10^4 K. Note that ρ_0 is fixed. .47

- R-critical fronts, $\rho_0 < \rho_1$.

$$\begin{aligned} T_1 &= \tfrac{\gamma(\gamma-1)}{(\gamma+1)}\tfrac{\mu_1\varepsilon_0}{k}, \qquad v_0 = \sqrt{\tfrac{(\gamma^2-1)\varepsilon_0}{m_H}}, \\ \tfrac{\rho_1}{\rho_0} &= \tfrac{\gamma+1}{\gamma}, \qquad \rho_0 = J\sqrt{\tfrac{m_H^3}{(\gamma^2-1)\varepsilon_0}}. \end{aligned} \tag{41}$$

  We have $\rho_1/\rho_0 = 8/3$ and $v_0 \sim 26$ km s^{-1}, so that the front is supersonic. Note that

$$v_0 = \sqrt{\frac{(\gamma^2-1)\varepsilon_0}{m_H}} = \rho_1 v_1/\rho_0 = \rho_1 c_1/\rho_0 = 8/3 c_1,$$

  the R front propagates at 8/3 ($\sim$ twice) the downstream sound speed. .48

[3] remember we are neglecting internal degrees of freedom, even for H_2

The precursor shock

- We see from both Eq. 40 and 41 that the upstream density ρ_0 is fixed by the ionising photon flux J and by ε_0, both of which are functions of the central star spectrum.
- ρ_0 is in general different from $\rho_{\rm ISM}$, the ambient density in which the shock progresses. The front is therefore preceded by a density (i.e. pressure) perturbation, which travels at the sound speed set by T_0.
- R-fronts are supersonic, so the precursor perturbation cannot travel away from the front.
- D-fronts are subsonic (~ 0.2 km s^{-1}), so the precursor perturbation can form a wave. Since ρ_0 is fixed by J, close to the central star (or early in the evolution of the H II region), $\rho_0 > \rho_{\rm ISM}$.
- In D-fronts the precursor wave will form a shock since the upstream gas is heated by the compression, so that $T_0 > T_{\rm ISM}$. An approximate quantitative descriptions of the shock can be found in Spitzer (1978)

.49

Evolution of H II regions

- Turn-on phase.
  An O star is suddenly turned-on in an infite and homogeneous medium, with a constant ionising photon luminosity S. Initially, for times short compared to the recombination timescale $\tau_{\rm rec} = (n_{\rm ISM}\alpha_2)^{-1} \approx 100$ yr for $n_{\rm ISM} = 10^3 {\rm cm}^{-3}$, all photons from the star lead to ionisation, and the star ionises a sphere of radius $r(t)$, such that

$$St = \frac{4\pi}{3} n_{\rm ISM} r^3(t).$$

  This sphere expands at a velocity

$$\frac{dr}{dt} = \frac{1}{3}\left(\frac{3S}{4\pi n_{\rm ISM}}\right)^{1/3} t^{-2/3},$$

  which at 100 yr is $\sim 4\ 10^3$ km s^{-1}. **this phase has never been observed, and the present description is unrealistic**. This phase is an R-front since the ionised gas is hotter and denser (factor of 2).

.50

- Approach to the Strömgren radius.
  Following the turn-on phase, at timescales of order $\tau_{\rm rec}$ we must take into account recombination so that the radius of the R-front is given by

$$\frac{dr}{dt} = \frac{1}{4\pi r^2 n_{\rm ISM}}\left[S - \frac{4}{3}\pi r^3 n_{\rm ISM}^2 \alpha_2\right],$$

  where we have used the on-the-spot approx. The solution to this equation is

$$r^3 = R_S^3[1 - \exp(-n_{\rm ISM}\alpha_2 t)],$$

where R_S is the Strömgren radius.
Thus the front velocity will progressively decrease until it reaches the 'R'-critical value, after which it will jump down to the 'D'-critical value (somewhere close to the Strömgren radius).

.51